Journal for ImmunoTherapy of Cancer

Defects in intratumoral arginine metabolism attenuate the replication and therapeutic efficacy of oncolytic myxoma virus

Parker Dryja,[1] Heather D Curtsinger,[2] Mee Y Bartee,[2] Eric Bartee [2]

To cite: Dryja P, Curtsinger HD, Bartee MY, *et al*. Defects in intratumoral arginine metabolism attenuate the replication and therapeutic efficacy of oncolytic myxoma virus. *Journal for ImmunoTherapy of Cancer* 2023;**11**:e006388. doi:10.1136/jitc-2022-006388

► Additional supplemental material is published online only. To view, please visit the journal online (http://dx.doi.org/10.1136/jitc-2022-006388).

Accepted 12 May 2023

[1]Program in Molecular and Cellular Biology and Pathobiology, Medical University of South Carolina, Charleston, South Carolina, USA
[2]Department of Internal Medicine, University of New Mexico Health Sciences Center, Albuquerque, New Mexico, USA

Correspondence to
Dr Eric Bartee;
ebartee@salud.unm.edu

ABSTRACT

Background Arginine (Arg) is a semiessential amino acid whose bioavailability is required for the in vitro replication of several oncolytic viruses. In vivo, Arg bioavailability is regulated by a combination of dietary intake, protein catabolism, and limited biosynthesis through portions of the urea cycle. Interestingly, despite the importance of bioavailable Arg to support cellular proliferation, many forms of cancer are functionally auxotrophic for this amino acid due to the epigenetic silencing of argininosuccinate synthetase 1 (ASS1), an enzyme responsible for the conversion of citrulline and aspartate into the Arg precursor argininosuccinate. The impact of this silencing on oncolytic virotherapy (OV), however, has never been examined.

Methods To address this gap in knowledge, we generated tumor cells lacking ASS1 and examined how loss of this enzyme impacted the in vivo replication and therapeutic efficacy of oncolytic myxoma virus (MYXV). We also generated a series of recombinant MYXV constructs expressing exogenous ASS1 to evaluate the therapeutic benefit of virally reconstituting Arg biosynthesis in ASS1$^{-/-}$ tumors.

Results Our results show that the in vitro replication of oncolytic MYXV is dependent on the presence of bioavailable Arg. This dependence can be overcome by the addition of the metabolic precursor citrulline, however, this rescue requires expression of ASS1. Because of this, tumors formed from functionally ASS1$^{-/-}$ cells display significantly reduced MYXV replication as well as poorer therapeutic responses. Critically, both defects could be partially rescued by expressing exogenous ASS1 from recombinant oncolytic MYXVs.

Conclusions These results demonstrate that intratumoral defects to Arg metabolism can serve as a novel barrier to virally induced immunotherapy and that the exogenous expression of ASS1 can improve the efficacy of OV in Arg-auxotrophic tumors.

WHAT IS ALREADY KNOWN ON THIS TOPIC

⇒ Arginine (Arg) is known to be required for the replication of numerous oncolytic viruses, and the metabolism of this amino acid is known to be dysregulated in numerous forms of cancer. However, the impact of dysregulated Arg metabolism on oncolytic virotherapy (OV) has never been studied.

WHAT THIS STUDY ADDS

⇒ Here we show that the loss of argininosuccinate synthetase 1 (ASS1) from malignant cells directly inhibits the efficacy of MYXV-based OV and that these defects may be overcome through viral reconstitution of Arg biosynthesis. These data suggest that dysregulated amino acid metabolisms within the tumor microenvironment can play a major role in determining the outcomes of OV.

HOW THIS STUDY MIGHT AFFECT RESEARCH, PRACTICE OR POLICY

⇒ This work suggests that inclusion of ASS1 into recombinant oncolytic viruses could improve efficacy against Arg-auxotrophic tumors as well as that ASS1 status might represent a novel prognostic factor to determine which patients might respond to OV.

INTRODUCTION

Oncolytic virotherapy (OV) represents a class of immunotherapeutics that employs a spectrum of live, replicating viruses to treat a variety of cancer types. The clinical impact of OV occurs through two main mechanisms. For some viruses, efficacy is mediated primarily through direct lytic potential, with tumor regression resulting from the rapid destruction of directly infected malignant cells. For other viruses, efficacy is driven primarily by the virally initiated recruitment of antitumor immune cells.[1] Fundamentally, however, both of these mechanisms typically rely on the productive replication and spread of the oncolytic agent within treated tumors. Understanding the factors that influence this replication is therefore essential to completely appreciating how OV functions.

Outside of the context of OV, it is well established that all viral replications rely on host metabolism. Because of this, the ways in which viruses hijack and manipulate host metabolic pathways to support viral infection are broadly studied.[2–6] Several pathways

such as tricarboxylic acid anaplerosis and associated glycolysis, glutaminolysis, and fatty acid synthesis, are frequent targets of viral effector proteins which function to sustain the anabolic synthesis of metabolites required for viral replication. For example, human cytomegalovirus directly increases glucose import by causing preferential expression of the higher affinity GLUT4 over GLUT1,[7] while human adenovirus type 5 alters glucose metabolism and drives glutaminolysis through activation of MYC.[8] Unlike the healthy tissues viruses have evolved to infect, however, metabolism within the tumor microenvironment (TME) is markedly different.[9–11] Indeed, widespread metabolic dysregulation is considered one of the fundamental hallmarks of cancer.[12] Interestingly, while the variety of specific metabolic defects that have been defined in cancer is extensive, some defects recur with unusual frequency. For example, a wide variety of cancers, including hepatocellular carcinoma, renal carcinoma, osteosarcoma, prostate cancer, pancreatic cancer, and melanoma, have been shown to epigenetically silence expression of the urea cycle enzyme argininosuccinate synthetase 1 (ASS1).[13] Loss of this enzyme prohibits cells from synthesizing their own arginine (Arg), making them entirely reliant on exogenous Arg or protein catabolism to maintain their cellular amino acid pools.

Despite the existing bodies of literature separately defining the metabolic dependencies of viruses as well as the metabolic dysregulations within the TME, studies into the impact of altered intratumoral metabolism on OV performance remain lacking. Given the complete dependence of oncolytic viruses on intratumoral metabolism as well as the possible overlap between viral Arg requirements and the development of Arg auxotrophy within solid tumors, we hypothesized that dysregulated Arg metabolism might impart resistance to OV by limiting viral replication. In the current work, we test this hypothesis by examining how the tumor-intrinsic loss of ASS1 influences oncolytic MYXV replication and therapeutic performance in various murine tumor models.

METHODS

Cell lines and reagents

Both the BSC40 and B16F10 cells lines were purchased from the American Type Culture Collection (Manassas, Virginia, USA). Lewis lung Carcinoma-A9F1 cells (A9F1)[14] were a generous gift from Dr Mark Rubinstein at the Medical University of South Carolina. ASS1^{KO} B16F10 cell lines were generated using a CRISPR/Cas9 system targeting murine ASS1 (gRNA sequence: TCAGGCCAACATTGGCCAGA, plasmid: PX459; GenScript, Piscataway, New Jersey, USA) as previously described.[15 16] B16F10 cells treated with a scrambled gRNA (referred to in this article as wild-type (WT) cells) have been previously described.[15] Cell lines were maintained in complete Dulbecco's Modified Eagle Medium (DMEM) (Corning, Corning, New York, USA) supplemented with 10% fetal bovine serum (FBS) (VWR, Radnor, Pennsylvania, USA) and 1× penicillin/streptomycin/glutamine (Corning). The FBS lot used in this study did not contain functionally relevant levels of residual Arg or citrulline (online supplemental figure S1). Media lacking each amino acid was created by starting with DMEM lacking all essential amino acids (United States Biological, Salem, Massachusetts, USA) and supplementing it with all the amino acids typically found in DMEM (Sigma-Aldrich, St. Louis, Missouri, USA), barring the amino acid of interest. Media specifically lacking Arg (–Arg) was created by starting with DMEM lacking Arg (United States Biological) and supplementing it with 3.7 g/L sodium bicarbonate and the specified concentrations of filter-sterilized L-Arg-HCl (VWR). Arg-free media reconstituted with 400 µM L-Arg-HCl were used for all control conditions. For metabolic rescue, Arg-free media were supplemented with either 400 µM L-citrulline or argininosuccinate (AS) (Sigma-Aldrich). For all in vitro experiments involving –Arg groups and MYXV infection, cells were cultured in –Arg media 24 hours prior to infection. Cultures were checked quarterly for mycoplasma contamination using PCR. The following primary antibodies were used for western blotting in this study: ASS1 (D404B; Cell Signaling Technology, Danvers, Massachusetts, USA); ornithine transcarbamylase (OTC) (NBP1-31582; Novus Biologicals, Centennial, Colorado, USA); argininosuccinate lyase (ASL) (NBP1-32752, Novus Biologicals); and β-actin (13E5, Cell Signaling Technology). Horseradish Peroxidase (HRP)-linked anti-rabbit IgG (7074S, Cell Signaling Technology) was used as the secondary antibody for all blots.

Viral constructs, infection, and quantification of virus

All constructs used in the current article are based on the Lausanne strain of MYXV.[17 18] Recombinant myxoma virus-expressing green fluorescent protein (MyxGFP) has been previously described.[16 19] Constructs generated within this article include MYXV encoding full-length murine ASS1 (MyxASS1), MYXV encoding a non-functional, frame-shifted murine ASS1 (MyxASS1^{FS}), and MYXV encoding the soluble ectodomain of murine PD1, an interleukin (IL)-12 fusion protein, and full-length murine ASS1 (MyxPD1/IL-12/ASS1). To generate MyxASS1 and MyxASS1^{FS}, BSC40 cells were transfected with a pBluescript plasmid encoding both green fluorescent protein (GFP) and the murine ASS1 open reading frame (ORF) located between fragments homologous to the MYXV *m135r* and *m136r* genes. MyxASS1 was generated using the intact murine ASS1 ORF, while MyxASS1^{FS} was generated using an ASS1 ORF lacking the first 85 base pairs (which deletes the start codon and also introduces a frameshift). Cells were then infected with MYXV–Lausanne, and clonal, recombinant viruses expressing GFP were isolated as previously described.[19] MyxPD1/IL-12/ASS1 was generated through a two-step process. In the first step, BSC40 cells were transfected with a pBluescript plasmid encoding both GFP and a fusion protein encoding the soluble ectodomain of murine PD1 (aa 1–167) linked to an IL-12 (p35-p40 fusion) by a P2A

self-cleaving peptide linker located between fragments homologous to the MYXV *m152r* and *m154r* genes. Cells were then infected with MYXV–Lausanne, and clonal recombinant viruses expressing GFP were isolated as previously described.[19] In the second step, BSC40 cells were transfected with a pBluescript plasmid encoding both mKATE and the murine ASS1 ORF located between fragments homologous to the MYXV *m135r* and *m136r* genes. Cells were then infected with the previously generated MyxPD1/IL-12 construct, and clonal recombinant viruses expressing mKATE were isolated as previously described.[19] Following clonal isolation, all constructs were amplified in BSC40 cells and purified using gradient centrifugation as previously described.[20] For all in vitro infections, the desired amount of virus was added directly to cell cultures without media exchange so as not to disturb existing Arg content within the culture. To quantitate infectious virus (from all in vitro and in vivo samples as well as produced viral stock), cell pellets from either cell culture or infected tumor samples were freeze-thawed over three cycles in liquid nitrogen and a 37°C water bath. Pellets were frozen a fourth time in liquid nitrogen and then thawed/sonicated for 3 min. Resulting homogenates were serially diluted and plated onto confluent BSC40s. The number of GFP^+ foci was then quantified 48 hours post infection and used to determine the titer of original samples.

MTT assay

Cells were plated at 10% confluency in a 96-well plate and left to incubate for 24 hours post splitting. Media were then exchanged with either control, +citrulline/−Arg, +AS/−Arg, or −Arg media where applicable. At the indicated time points, MTT substrate (CellTiter 96 Non-Radioactive Cell Proliferation Assay; Promega, Madison, Michigan, USA) was added at a 1:100 ratio to each well, and plates were incubated for 1.0–1.5 hours at 37°C. Stop solution of 100 µL was then added and the well contents were homogenized via repeated pipetting. Total absorbance at 595 nm was then measured on a BioTek Synergy Neo2 Plate Reader.

Mouse models

Female C57Bl/6J mice aged 6–10 weeks were obtained from Jackson Laboratories (Bar Harbor, Massachusetts, USA) and seeded subcutaneously with 1×10^6 tumor cells in 50 µL of cold phosphate-buffered saline (PBS). Tumors were allowed to establish until they reached ~25 mm^2 prior to use. Mice that did not establish consistent tumors were removed before the initiation of the experiment. In experiments evaluating viral replication and infection burden, mice were treated with a singular dose of 1×10^6 foci-forming units (FFUs) of the indicated MYXV construct injected intratumorally in 50 µL of PBS. In experiments measuring therapeutic response, mice were treated with three doses of 1×10^5 FFU of the indicated MYXV construct injected intratumorally in 50 µL of PBS. This dose was selected as previous experiments indicated that it yields tumor control but infrequent cures, making it an ideal starting point to compare gain or loss of therapeutic response. Therapeutic doses were administered every other day over 5 days. Mice were euthanized when their tumor area exceeded 400 mm^2 (determined by measuring length×width with digital calipers). For all in vivo experiments, each data point represents a singular sample taken from an individual mouse bearing a single tumor. All experiments were approved by the University of New Mexico Health Science Center institutional animal care and use committee under protocol #20-201002-HSC.

Histology

Tumors harvested from mice at the specified times were sagittally bisected with a scalpel, embedded in optical coherence tomography media, and frozen in liquid nitrogen-chilled isopentane for cryosectioning. Sections of tumors were cut on a cryostat at 8 µm section thickness. One section per tumor was taken for quantification. Images were collected on an Evos M5000 microscope using a GFP filter cube. Final images were used to quantify infection area, foci count, and foci characteristics in Fiji.[21]

Metabolomics

For metabolic analysis of virally treated tumors, B16F10 tumors were established on syngeneic C57Bl/6J mice for 7 days. Tumors were then treated with a single dose of 1×10^6 FFU of MyxGFP delivered directly intratumorally. Tumors were harvested 4 days post viral treatment (day 11 post initial implantation) and processed for analysis. For metabolic analysis of $ASS1^{WT}$ and KO tumors, B16F10 tumors were established on syngeneic C57Bl/6J mice. Tumors were harvested 11 days after implantation and processed for analysis. For processing, tumors were immediately snap-frozen in liquid nitrogen at point of harvest. Frozen tumors were weighed and then broken into coarse homogenates using mechanical percussion in liquid nitrogen-cooled vessels. Frozen coarse homogenates of 30–50 mg were then suspended in 80% methanol at 20 µL/mg tissue. Suspensions were sonicated, centrifuged at 12 000×*g*, and the resulting supernatants were analyzed via liquid chromatography–mass spectrometry by the Metabolomics Core Facility at Robert H. Lurie Comprehensive Cancer Center of Northwestern University (Chicago, Illinois, USA) as previously described.[22] Metabolites without separable peaks or with unconfirmed identities were pruned prior to analysis (304 species down to 226 species, input list as seen in online supplemental table S1); samples were normalized against total ion current; and comparisons were drawn between groups across the peak area. Analysis of metabolomics data was performed using metaboanalyst[23] on $\log_{10}$-transformed datasets with autoscaling (mean centered, divided by the SD of each variable). Global Test and relative-betweeness centrality were selected for enrichment method and topology analysis, respectively. The list of entries seen in

online supplemental table S1 was used as the reference metabolome for pathway analysis.

Statistical and informatic methods

Principal component analyses were performed in R V.4.0.2 using the ggbiplot package for visualization. All other statistical analyses were performed in the Statistical Package for the Social Sciences. For statistical tests comparing two groups, unpaired Student's t-tests were used to determine significance (α=0.05). For statistical tests comparing more than two groups, analyses of variance with Tukey's honestly significant difference (Levene $p<0.05$) or Games-Howell (Levene $p<0.05$) post hoc tests were used to determine significance (α=0.05). Differences in animal survival were determined using log-rank analysis ($p<0.05$). The specific test used for each analysis is notated within the figure legend. All error bars indicate the SEM unless noted otherwise in figure legends.

RESULTS

MYXV replication is dependent on bioavailable Arg

OV frequently relies on the replication of the oncolytic agent within treated tumors. Additionally, it is well established that all viral replications depend on the metabolic state of their host cells. However, relatively few studies have examined how intratumoral metabolism (particularly outside the context of energetics) might impact OV. To begin to address this issue, we first made the assumption that viral infection would likely alter metabolic pathways which were critical to successful replication. Based on this assumption, we next sought to identify metabolic pathways which might be critical to the in vivo replication of oncolytic MYXV by assaying changes to intratumoral metabolites following viral treatment. To do this, B16F10 tumors were established on syngeneic mice and then treated with a single bolus of PBS or 1×10^6 FFU of MyxGFP. Four days post treatment, tumors were harvested, and the abundance of various hydrophilic metabolites was analyzed using whole tissue metabolomics. Metabolite set enrichment analysis of the resulting dataset revealed that viral treatment altered numerous metabolic pathways involved in amino acid metabolism including Arg, proline, glycine, serine, threonine, cysteine and methionine, suggesting that these pathways might play a crucial role in MYXV infection (figure 1A). Consistent with this hypothesis, removal of numerous amino acids from cellular growth media significantly reduced the numbers of infectious MYXV progeny produced in B16F10 cells in vitro (figure 1B). Notably, of all the amino acids tested, removal of Arg had the most potent inhibitory effect on viral yields in vitro, and Arg metabolism was the most highly altered metabolic pathway identified by our in vivo metabolic screen with virally treated tumors displaying reduced abundance of the urea cycle precursor L-citrulline as well as increased abundance of the downstream products ornithine, putrescine, and spermine (figure 1C). Consistent with Arg being generally essential for MYXV replication, removal of exogenous Arg from cell culture media resulted in a dramatic reduction in the abundance of virally derived GFP (figure 2A) and little to no production of new infectious viral particles at any time post infection (figure 2B) in multiple cell lines including malignant B16F10 and A9F1 cells as well as the non-malignant line BSC40. These changes could not be explained by a general loss of cellular viability since Arg deprivation resulted in cytostasis but did not appear to acutely kill cells over the duration of these experiments (online supplemental figure S2). Titrations of exogenous Arg into culture media revealed a strong dose dependency between the production of new infectious MYXV progeny and the bioavailability of this amino acid in all three cell lines with maximal viral replication occurring at concentrations ≥100 µM and a consistent EC_{50} of ~50 µM (figure 2C). Critically, this EC_{50} is within the physiological range of Arg, which has been reported to be between 50 µM and 150 µM in the serum of healthy mice.[24–26] Taken together, these data suggest that Arg metabolism might play a critical role in the in vitro and in vivo replication of oncolytic MYXV.

Intrinsic Arg biosynthesis can support MYXV replication in ASS1-competent cells

In the absence of exogenous Arg, many cells can directly biosynthesize this amino acid through a portion of the urea cycle. This biosynthesis requires the primary metabolic precursors citrulline and aspartate, as well as expression of the urea cycle enzymes ASS1 and ASL (figure 1C). Since our previous studies had demonstrated that MYXV replication required bioavailable Arg, we next asked whether intrinsic Arg biosynthesis could rescue viral replication when this amino acid was not exogenously available. To test this, we first evaluated expression of the three major urea cycle enzymes in B16F10 and A9F1 cells using western blotting. The results demonstrated that, despite previous reports suggesting that ASS1 is frequently silenced in human melanomas, the murine-lineage B16F10s evaluated here expressed both ASS1 and ASL (figure 3A). In contrast, A9F1s were found to be deficient in ASS1 expression. Not surprisingly, neither cell line expressed detectable levels of OTC, which is typically only found in the liver. In agreement with these phenotypical results, the cytostasis induced in B16F10s by removal of Arg could be partially rescued by supplementation with exogenous citrulline (figure 3B), suggesting that these cells were functionally Arg-autotrophic. In contrast, cytostasis of the intrinsically $ASS1^{-/-}$ A9F1 cells could not be rescued by citrulline (figure 3B). Critically, citrulline supplementation could also rescue MYXV replication in B16F10 cells but not A9F1 cells (figure 3C), suggesting that intrinsic Arg biosynthesis is sufficient to support MYXV replication in the absence of exogenous Arg but that this rescue requires expression of ASS1.

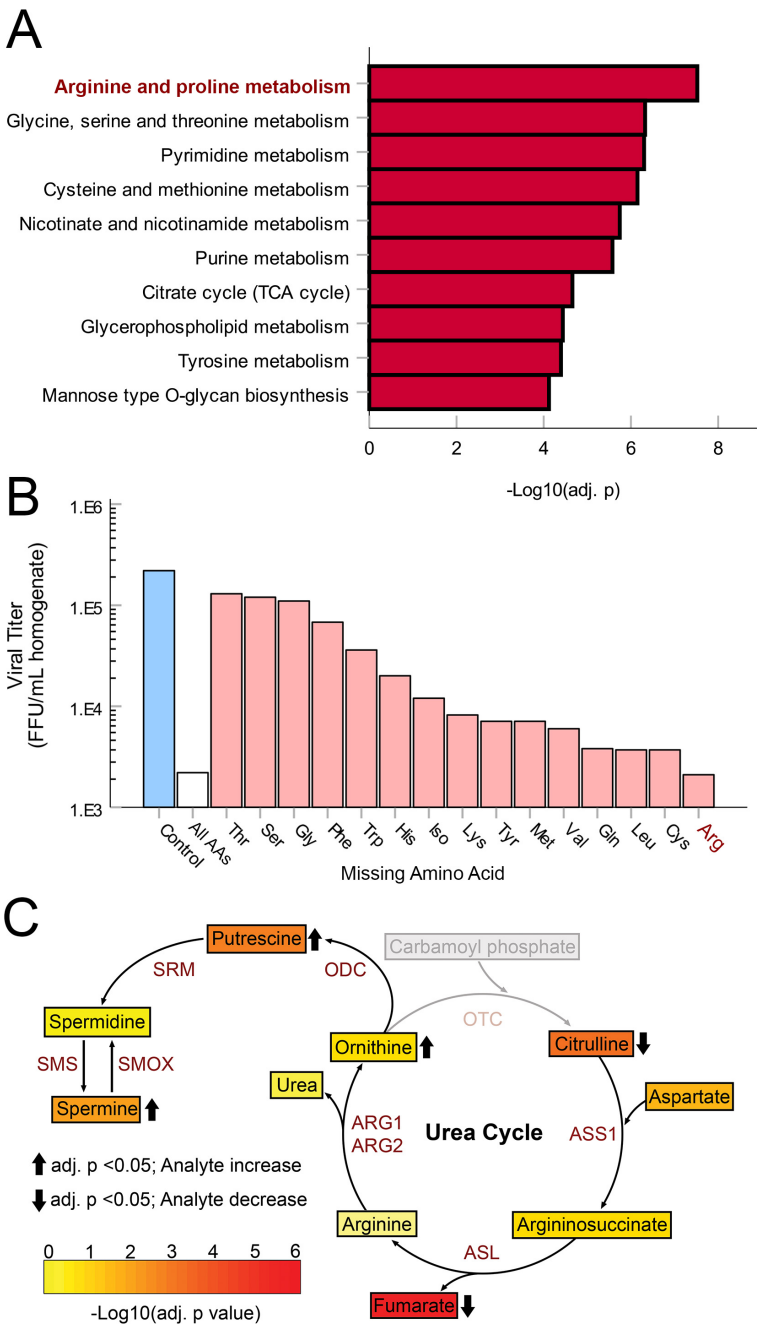

Figure 1 MYXV infection alters the Arg biosynthetic pathway: B16F10 tumors established in C57BL/6J mice were treated with either PBS or MyxGFP. Four days post treatment, tumors were harvested and immediately snap-frozen in liquid nitrogen. Whole-tumor homogenates were then used to quantify a set of 226-metabolite species via LC-MS (n=5–7 tumors per group). (A) Metabolite set enrichment analysis of LC-MS results. (B) Viral yields from B16F10 cells grown in DMEM lacking various single amino acids for 24 hours and infected with MyxGFP at an multiplicity of infection (MOI)=5. Cells were harvested 24 hours post infection for viral quantification. (C) Heatmap of metabolite concentrations involved in the urea cycle and polyamine biosynthesis from experiment (A). Color indicates $-\log_{10}$(Holm adjusted p value). Arrows indicate significant (Holm adjusted p value <0.05) increases or decreases in MyxGFP-treated cohort relative to mock cohort. Gray indicates species not evaluated in this panel. Arg, arginine; ASL, argininosuccinate lyase; DMEM, Dulbecco's Modified Eagle Medium; FFU, focus-forming unit; LC-MS, iquid chromatography–mass spectrometry; MyxGFP, myxoma virus-expressing green fluorescent protein; MYXV, myxoma virus; PBS, phosphate-buffered saline; ODC, ornithine decarboxylase; SRM, spermidine synthase; SMS, spermine synthase; SMOX, spermine oxidase.

Loss of ASS1 decreases MYXV replication both in vitro and in vivo

Arg bioavailability is thought to be limiting within many forms of solid tumors[9 11] and our previous results suggested that Arg biosynthesis might play a major role in determining the outcomes of MYXV replication under these conditions. We therefore wanted to determine whether a tumor's ASS1-status might influence its

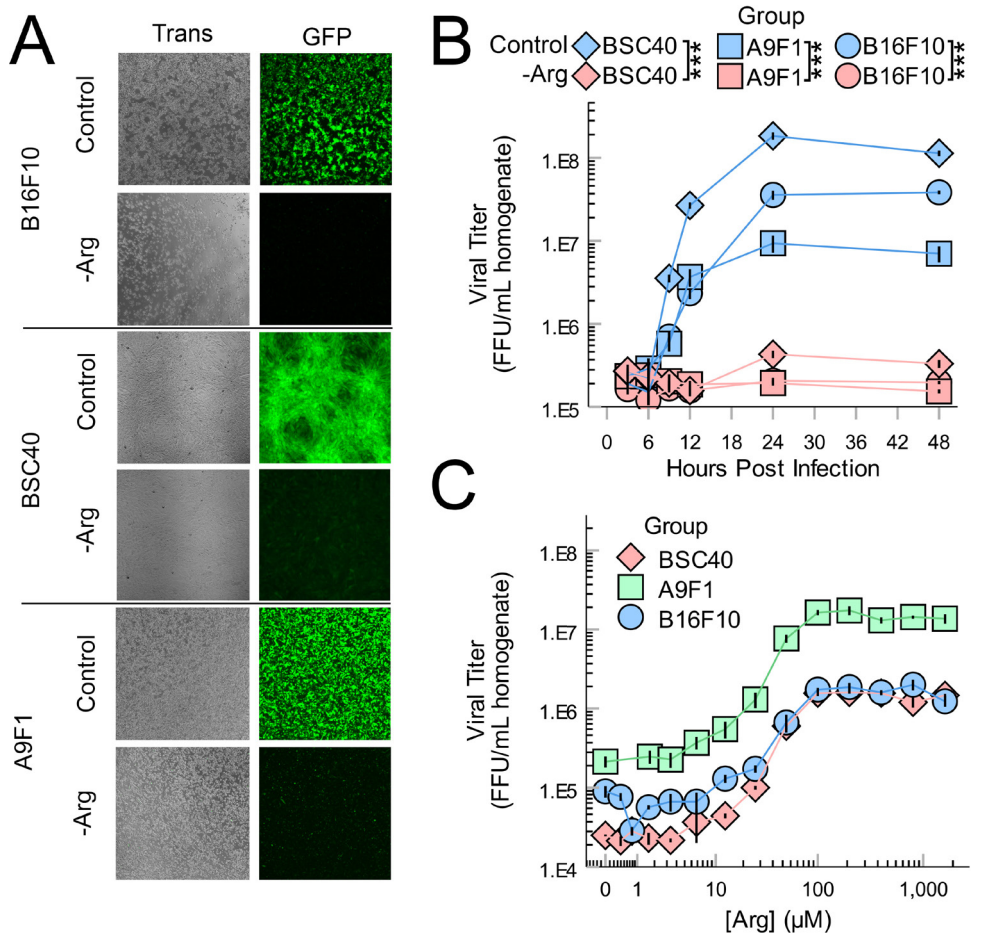

Figure 2 MYXV replication requires bioavailable Arg. (A) The indicated cells lines were incubated in complete media or media lacking Arg for 24 hours and then infected with MyxGFP at an MOI=5. Expression of virally derived GFP was visualized 24 hours post infection using flourescent microscopy. (B) The indicated cells were incubated in complete media or media lacking Arg for 24 hours and then infected with MyxGFP at an MOI=5. At the indicated times post infection, cells were harvested and the amount of infectious virus present was quantified using viral titration assays. Statistical significance was determined by unpaired Student's t-test on samples collected at 24 hours (n=3 per group, per cell line). (C) The indicated cells were incubated in a gradient of Arg-deficient DMEM for 24 hours prior to infection with MyxGFP at an MOI=5. Cells were harvested 24 hours post infection and the amount of infectious virus present was quantified using viral titration assays (n=3 per group, per cell line). ***P<0.001. Arg, arginine; DMEM, Dulbecco's Modified Eagle Medium; FFU, focus-forming unit; GFP, green fluorescent protein; MyxGFP, myxoma virus-expressing green fluorescent protein; MYXV, myxoma virus.

responsiveness to MYXV-based OV. To facilitate this study, we first generated a series of functionally ASS1-deficient B16F10 cell lines using CRISPR/Cas9 genome editing (online supplemental figure S3). These cell lines exhibited normal growth and morphology when cultured in standard DMEM but produced a truncated version of the ASS1 protein. Critically, both the cellular cytostasis and reduced MYXV replication induced by removal of Arg could no longer be rescued by the addition of citrulline in these cell lines but remained rescueable by the addition of the downstream metabolite AS demonstrating that these cells were now functionally ASS1-deficient. Additionally, tumors formed from these $ASS1^{KO}$ cells displayed metabolomic profiles consistent with defective Arg biosynthesis including significantly increased citrulline content and reduced levels of Arg (online supplemental figure S4).

Having generated functionally ASS1-deficient cell lines, we next sought to determine whether the loss of this enzyme might influence MYXV replication in vivo. Syngeneic mice were implanted subcutaneously with either $ASS1^{WT}$ or $ASS1^{KO}$ B16F10 cells. Seven days post implantation, the resulting tumors were treated with a single bolus of 1×10^6 FFU of MYXV. Six days after viral treatment, tumors were harvested and the rate of viral infection was determined both by visually assessing expression of virally derived GFP within tumor sections as well as by quantifying the abundance of infectious virions. Consistent with previous reports,[27 28] 6 days post-treatment, $ASS1^{WT}$ B16F10 tumors displayed numerous distinct GFP^+ regions corresponding to individual foci of infection (figure 4A,B) and contained high numbers of infectious MYXV particles (figure 4C). In contrast, tumors formed from two distinct $ASS1^{KO}$ clones displayed significantly reduced visual signs of infection (figure 4A,B) as well as a ~2 log reduction in infectious virus (figure 4C). Taken together, these results suggest that the loss of ASS1

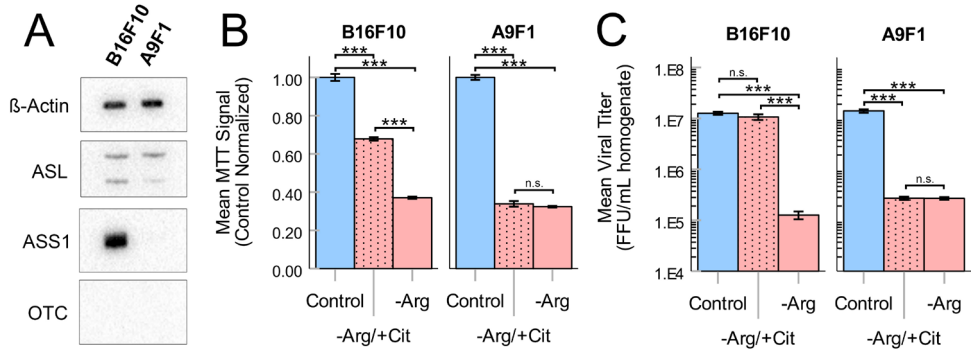

Figure 3 Intrinsic Arg biosynthesis can support MYXV replication in Arg limited conditions. (A) Western blots analyzing expression of the urea cycle components ASS1, ASL, and OTC in B16F10 and A9F1 cells. (B) MTT assays of B16F10 and A9F1 cells cultured for 24 hours in control DMEM (control), Arg-deficient media supplemented with 400 µM citrulline (–Arg/+Cit), or Arg-deficient media (–Arg). (C) The indicated cells were incubated as previously shown and then infected with MyxGFP at an MOI=5. Twenty-four hours post infection, the amount of infectious virus present was quantified using viral titration assays. Statistical significance (B,C) was determined by analysis of variance with Tukey's HSD post hoc test (n=3 per group, per cell line). ***P<0.001. Arg, arginine; ASL, argininosuccinate lyase; ASS1, argininosuccinate synthetase 1; DMEM, Dulbecco's Modified Eagle Medium; FFU, focus-forming unit; HSD, honest significant difference; MyxGFP, myxoma virus-expressing green fluorescent protein; MYXV, myxoma virus; n.s., no significance; OTC, ornithine transcarbamylase.

from malignant cells negatively impacts the replication of oncolytic MYXV in vivo by preventing intrinsic Arg biosynthesis.

Loss of ASS1 decreases the therapeutic response to MYXV-based OV

Previous work has suggested that oncolytic MYXV must replicate effectively within a tumor to induce therapeutic regression.[29 30] Since our previous analyses had suggested that loss of ASS1 severely compromised MYXV replication within treated tumors, we wished to determine whether these tumors might also display reduced responsiveness to MYXV-based OV. Since the therapeutic response of B16F10 tumors to unmodified MYXV is typically negligible,[16] in order to address this question, we established B16F10 tumors in syngeneic mice and then treated them with a recently described doubly recombinant MYXV construct which expressed both a PD1 inhibitor and IL-12 (MyxPD1/IL-12[16 19]) (figure 5A) whose replication was also found to be dependent on the bioavailability of Arg (online supplemental figure S5). Consistent with our previously observed reductions in viral replication, $ASS1^{KO}$ tumors treated with MyxPD1/IL-12 displayed a less pronounced response to viral therapy including earlier tumor relapse and poorer overall survival (figure 5B,C). Taken together, these data suggest that ASS1 status might significantly impact the responsiveness of tumors to MYXV-based OV by restricting intratumoral viral replication.

Viral reconstitution of Arg biosynthesis rescues both intratumoral replication and therapeutic efficacy

Since our previous data suggested that the tumor-intrinsic loss of ASS1 posed a barrier to both OV replication and

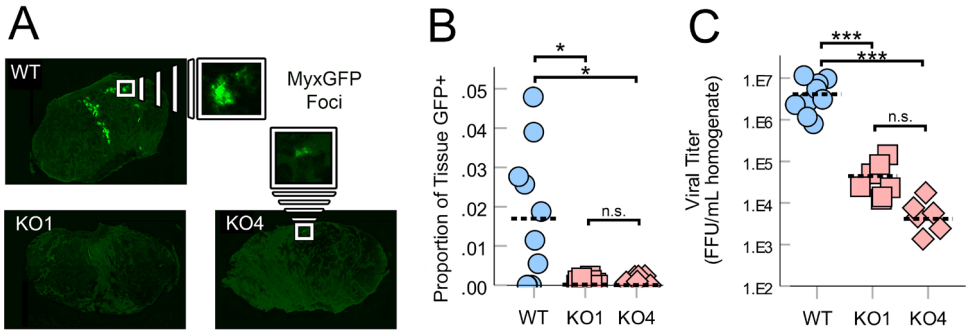

Figure 4 Loss of ASS1 reduces MYXV replication in vivo: $ASS1^{WT}$ or $ASS1^{KO}$ (KO#1 and KO#4) B16F10 tumors were established on C57Bl/6J mice and then treated with a single bolus of 1×10^6 FFU of MyxGFP. Six days post infection, tumors were harvested and processed for frozen sectioning and quantification of viral titer. (A) Images of tumor sections that displayed the median amount of infection within each cohort. GFP signal indicates area of infection. (B) Quantification of infection area in infected tissues (shown in A) displayed as a percent of total tumor area, which is GFP+. One section was taken for imaging per tumor/mouse (n=6–9 per group). Hashed bars indicate the mean value for each group. (C) Quantification of infectious virus present within tumors (n=6–9 per group). Hashed bars indicate the mean value for each group. Statistical significance (B,C) was determined by analysis of variance with Games-Howell post hoc test. *P<0.05, ***P<0.001. FFU, focus-forming unit; GFP, green fluorescent protein; MyxGFP, myxoma virus-expressing green fluorescent protein; MYXV, myxoma virus; n.s., no significance; WT, wild type.

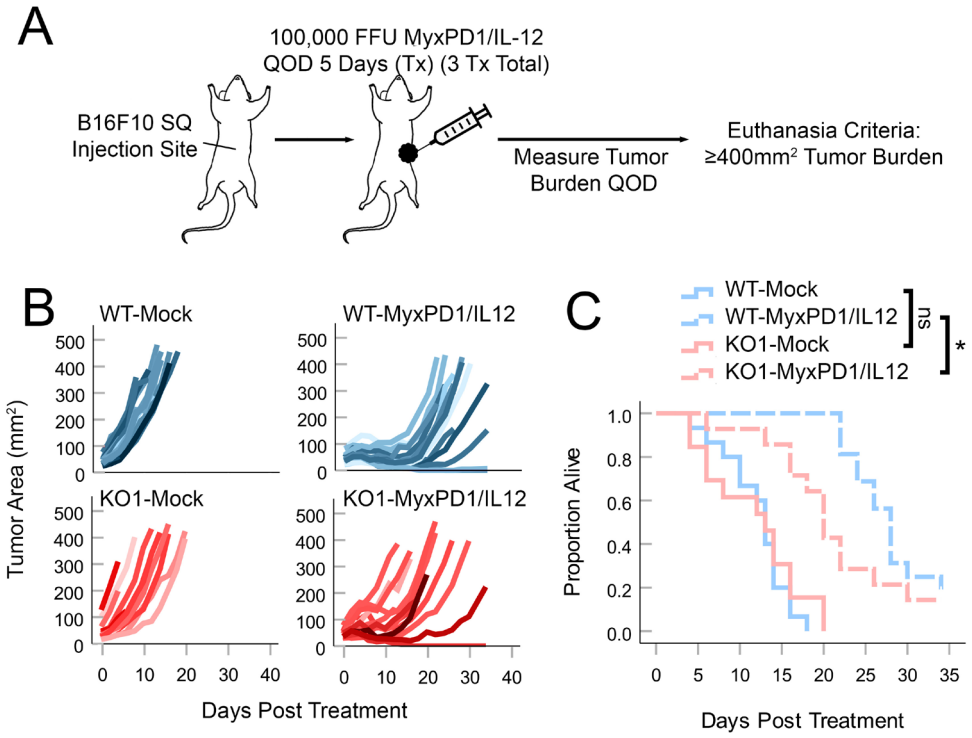

Figure 5 Loss of ASS1 blunts the therapeutic response to MYXV-mediated oncolytic virotherapy: ASS1^{WT} or ASS1^{KO} (KO#1) tumors were established in C57Bl/6J mice and then treated with three doses of either PBS (mock) or 1×10^5 FFU of MyxPD1/IL-12 intratumorally QOD over 5 days. Tumor burden was then monitored QOD in all cohorts. (A) Schematic of treatment regimen. (B) Spaghetti plots tracking individual tumor sizes over time. (C) Overall survival of mice. Statistical significance was determined using log-rank analysis. *P<0.05. Arg, arginine; ASS1, argininosuccinate synthetase 1; FFU, focus-forming unit; IL, interleukin; MYXV, myxoma virus; n.s., no significance; PBS, phosphate-buffered saline; QOD, every other day; WT, wild type.

therapeutic performance, we hypothesized that reconstituting the Arg biosynthetic pathway by expressing this enzyme from a recombinant MYXV might improve treatment of ASS1-deficient tumors. To address this, we generated a recombinant MYXV construct which expressed both GFP and the murine ASS1 ORF (MyxASS1) (figure 6A,B). A control virus expressing both GFP and a frameshifted portion of the murine ASS1 ORF (MyxASS1^{FS}) was also generated as a control. In vitro testing confirmed that the viral replication of both MyxASS1 and MyxASS1^{FS} was inhibited by the removal of Arg from the growth media. However, the replication of MyxASS1 could now be rescued in ASS1^{KO} B16F10 cells by the addition of citrulline, while the replication of MyxASS1^{FS} could not (figure 6C). Similarly, while MyxASS1 and MyxASS1^{FS} displayed similar viral titers in tumors derived from ASS1^{+} B16F10 cells, MyxASS1 displayed a strong trend towards increased viral titers in tumors derived from two distinct ASS1^{KO} B16/F10 cell lines (figure 6D) as well as significantly increased titers in tumors derived from intrinsically ASS1-deficient A9F1 cells (figure 6E). Finally, to determine whether expression of ASS1 might improve MYXV-based OV, we generated a triply recombinant, therapeutically active virus expressing full-length ASS1, along with soluble PD1 and IL-12 (MyxPD1/IL-12/ASS1) (figure 7A). Consistent with expression of ASS1 improving OV performance in Arg-auxotrophic tumors, treatment of tumors derived from ASS1^{KO} B16/F10 cells with MyxAss1/PD1/IL-12 resulted in improved tumor control compared with treatment with a non-ASS1 expressing control virus (figure 7B,C). Similar results were observed in mice bearing tumors derived from intrinsically ASS1-deficient A9F1 cells, although in this model the improvement of therapeutic efficacy presented as a higher percentage of complete responders and not an increase in median survival time (figure 7B and C). Collectively, these results demonstrate that defects to oncolytic virus replication and performance induced by the loss of ASS1 expression from malignant tumor cells may be, at least partially, overcome by the reconstitution of this pathway using recombinant viruses.

DISCUSSION

The efficacy of most OVs is influenced by the successful replication of the viral agent. However, despite this dependence, the barriers to this replication imposed by the TME remain incompletely understood. Previous work has clearly established that an intact antiviral response represents one major obstacle to achieving effective infection within treated tumors.[31 32] However, even within the context of severe immunodeficiency, such as immune deficient NOD.Cg-Prkdc/scid/Il2rg$^{tm1Wjl/Sz}$J mice, many oncolytic infections—including MYXV—still fail to achieve complete tumor eradication.[33] These data suggest that barriers to viral infection exist beyond the context

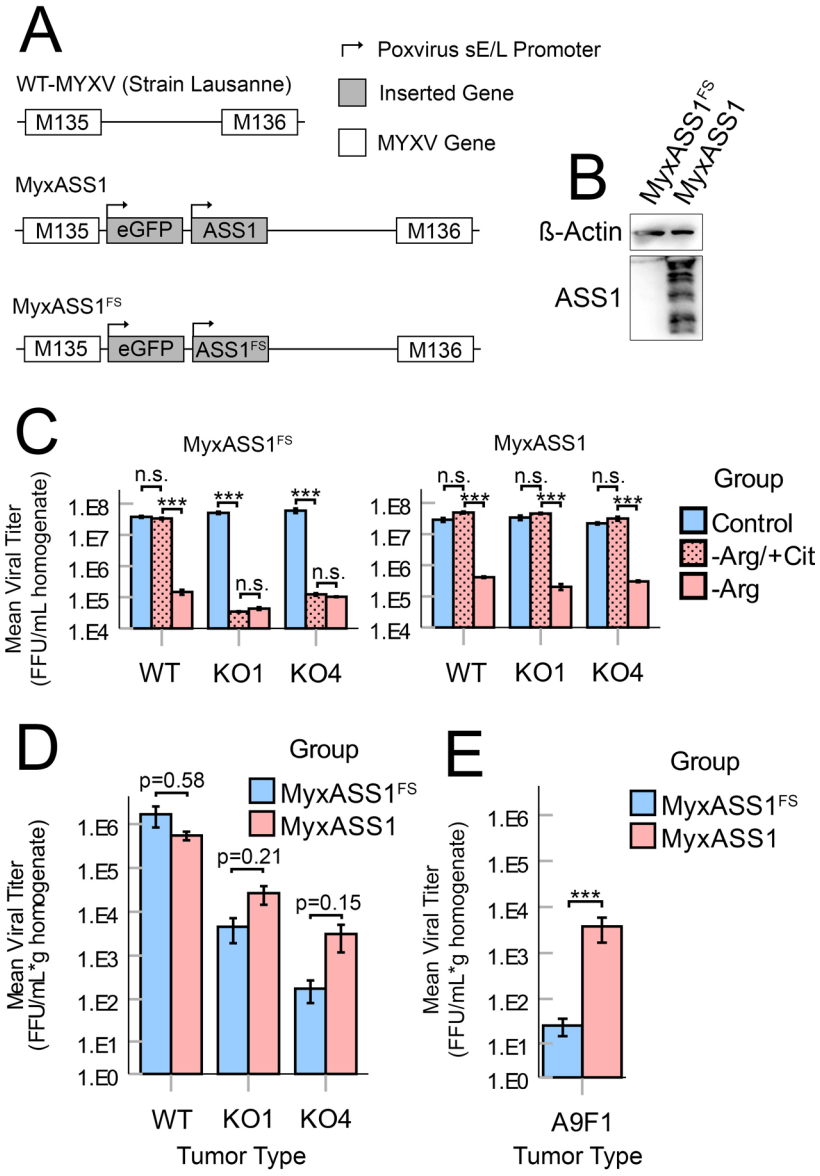

Figure 6 Expression of exogenous ASS1 from a recombinant MYXV improves viral replication in ASS1$^{-/-}$ tumors: (A) genomic schematic of recombinant viruses used in this study including MyxASS1 and MyxASS1^{FS}. (B) Expression of murine ASS1 in BSC40 cells infected with either MyxASS1 or MyxASS1^{FS} for 24 hours. (C) The indicated cells were incubated in complete media, –Arg media, or –Arg media supplemented with citrulline for 24 hours and then infected with either MyxASS1^{FS} (left) or MyxASS1 (right) at an MOI=5. Twenty-four hours post infection, cells were harvested and the amount of infectious virus present was quantified using viral titration assays. Statistical significance was determined by unpaired Student's t-test (n=3 per group, per cell line). (D) ASS1^{WT} and ASS1^{KO} (KO#1 and KO#4) tumors were established in C57Bl/6J mice. Tumors were then treated with a single bolus of 1×10^6 FFU of either MyxASS1 or MyxASS1^{FS}. Six days post infection, tumors were harvested and the abundance of infectious virus was quantified using viral titer assay (n=3–6 tumors per group). Statistical significance determined by unpaired Student's t-test (specific p values given). (E) A9F1 tumors were established in C57BL/6J mice and treated (as in D). Statistical significance was determined by unpaired Student's t-test (n=5–6 tumors per group). ***P<0.001. Arg, arginine; ASS1, argininosuccinate synthetase 1; FFU, focus-forming unit; MyxASS1, MYXV encoding full-length murine ASS1; MyxASS1^{FS}, MYXV encoding a non-functional, frame-shifted murine ASS1; MYXV, myxoma virus; n.s., no significance; WT, wild type.

of antiviral immunity. Determining the identity of these barriers therefore represents an opportunity to improve our basic understanding of OV as well as enhance its therapeutic potential. In this context, our results suggest that metabolic deficiencies resulting from dysregulation of Arg biosynthesis within malignant cells may contribute to OV resistance.

Our metabolomic evaluation of the changes induced in B16F10 tumors by viral treatment (figure 1) demonstrated clear changes to the Arg biosynthetic pathway on MYXV infection. This is consistent with recently published data suggesting that in vitro infection with MXYV induces significant changes to the amino acid profiles of cells.[34] While there are disparities in the magnitude of the

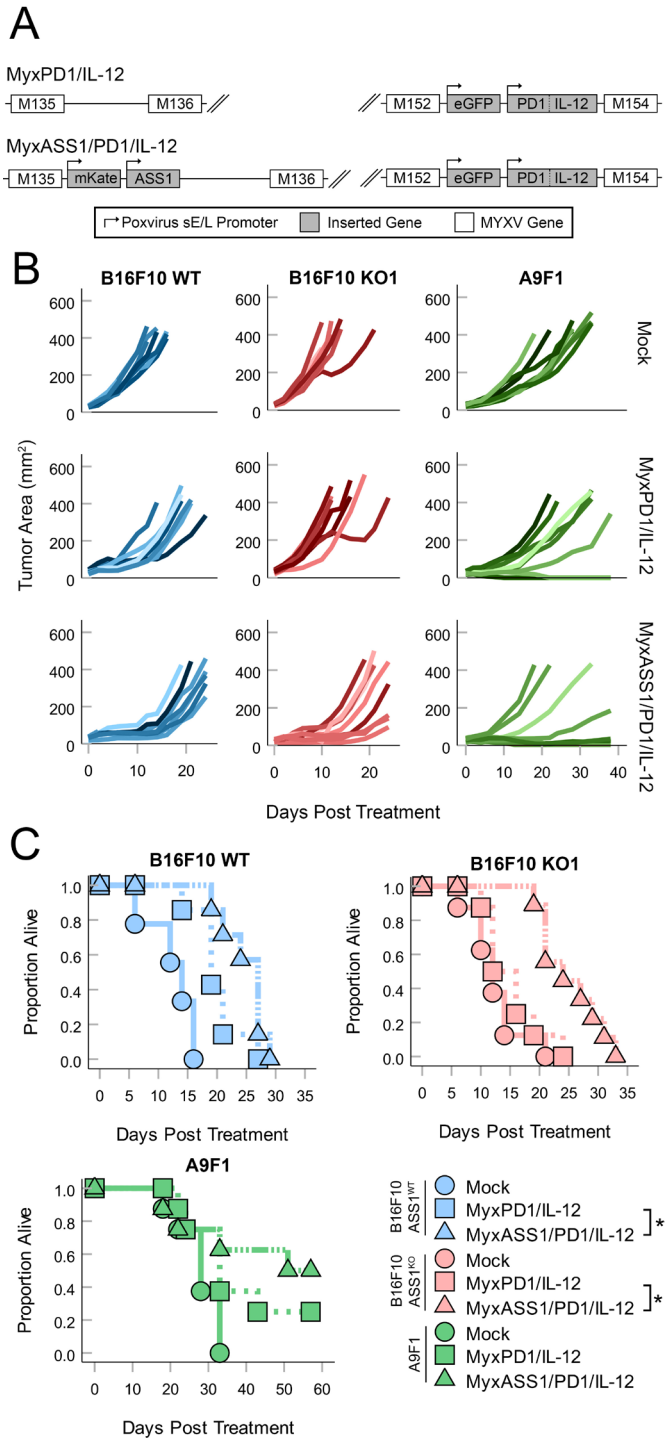

Figure 7 Expression of ASS1 improves MYXV-based OV. (A) Genomic schematic of recombinant viruses used in this study including MyxPD1/IL-12 and MyxASS1/PD1/IL-12. (B,C) ASS1^{WT}, ASS1^{KO} (KO#1 and KO#4), and A9F1 tumors were established in C57Bl/6J mice and then treated with three doses of either PBS (mock) or 1×10^5 FFU of MyxPD1/IL-12 or MyxASS1/PD1/IL-12 intratumorally QOD over 5 days. Tumor burden was then monitored QOD in all cohorts. (B) Spaghetti plots tracking individual tumor sizes over time. (C) Overall survival of mice. Statistical significance was determined using log-rank analysis (n=6–9 mice per group). *P<0.05. ASS1, argininosuccinate synthetase 1; IL, interleukin; MyxASS1, MYXV encoding full-length murine ASS1; MYXV, myxoma virus; OV, oncolytic virotherapy; PBS, phosphate-buffered saline; QOD, every other day; WT, wild type.

changes observed in our work and the previous study, these differences are likely attributable to the variable nature of the two systems used. For example, the in vitro conditions studied in the previous work are replete with all necessary nutrients to accommodate cell growth and viral replication and offer a highly contrasting metabolic landscape to established in vivo tumors. Furthermore, the previous work demonstrated that the degree of MYXV-induced metabolome remodeling was partially contingent on the cell line in question, making direct

comparisons between the works difficult. Despite these issues, it appears that both datasets support the overall conclusioin that amino acid metabolism likely plays a key role in supporting MYXV replication.

Similarly, consistent with previous reports on the related poxvirus vaccinia,[35 36] our in vitro data clearly demonstrate that MYXV infection is wholly dependent on the presence of bioavailable Arg in multiple cell lines (figure 2). While this observation is not surprising, it is important to point out that neither our current results nor the previous studies identify the specific mechanisms through which a lack of bioavailable Arg impacts poxviral replication. One potential model is that lack of Arg simply prevents effective translation of viral proteins by eliminating a required protein building block. While this model is conceptually attractive, preliminary studies suggest that cells starved of Arg do not acutely lose viability, while cells treated with the translational blocker cyclohexamide do (our unpublished observations, MYB 2023). Similarly, removal of Arg from growth media induces an unfolded protein response in cells which is highlighted by the *increased* translation of specific proteins such as ATF4.[37] These findings both argue that factors beyond a simple lack of protein building blocks may be playing a role. One alternative model is that the lack of Arg activates the integrated cellular stress response. In the context of amino acid starvation, this response is triggered by uncharged tRNAs causing activation of EIF2AK4 (known as GCN2 in mice). This activation subsequently blocks protein translation by phosphorylating eIF2α.[16 38] This response is similar to that induced by activation of the dsRNA sensor PKR, which has a well-studied role as an antiviral cellular response.[39] Similarities between the overall responses to amino acid starvation and viral infection may therefore create a scenario where lack of Arg induces a cellular state sufficiently overlapping with an antiviral response to inhibit viral replication. This notion is reinforced by evidence that EIF2AK4 is activated in some virally infected cells, implying a role for this pathway within a genuine antiviral response[40–43]; however, compared with the interaction of viruses with PKR, how the cellular response to amino acid starvation might be influenced by viral infection remains under studied. A final model is that Arg deprivation indirectly influences AKT phosphorylation by altering the mammalian target of rapamycin complex 1 and 2 (mTORC1:mTORC2) complex ratio through activation of the Castor complex.[44] Since MYXV replication is dependent on AKT phosphorylation, this change in mTORC could reduce viral infection. Interestingly, this last model predicts a unique impact of Arg deprivation on MYXV replication since most other oncolytic viruses are not dependent on the phosphorylation of AKT. Further studies in the mechanisms through which Arg deprivation inhibits the replication of MXYV (and other potential oncolytic candidates) therefore seem warranted.

Regardless of the precise mechanisms responsible for inhibiting MYXV replication in Arg-limited conditions, ASS1 competency had a clear, robust effect on both viral replication and therapeutic efficacy in vivo (figures 3–5). This suggests that bioavailable Arg is inherently limiting within the TME of both B16F10 and A9F1 tumors and that enough citrulline is present to allow for Arg biosynthesis in Arg-autotrophic cells. Unfortunately, neither our present work nor previously published studies examining the role of Arg in antitumor immunity have been able to directly confirm these hypotheses. Interestingly, even in $ASS1^{KO}$ tumors, some evidence of MYXV replication was still observed (figure 5). This replication occurred in significantly fewer distinct viral foci, with the majority being much smaller and dimmer than their counterparts in $ASS1^{WT}$ tumors. However, a few foci in $ASS1^{KO}$ tumors were individually comparable in size and GFP intensity to those found in $ASS1^{WT}$ tumors. While not definitive, this observation seems to suggest that loss of ASS1 functions by decreasing the portion of a tumor that is amenable to infection. These results potentially indicate that Arg bioavailability could be heterogeneous throughout the tumor and, if so, recapitulate our observations in vitro that infection can proceed unabated in $ASS1^{KO}$ cell lines so long as Arg is available exogenously. Unfortunately, preliminary attempts to spatially quantify Arg content within tumors via matrix-assisted laser desorption ionization as a mass spectrometry imaging (MALDI-MSI - our unpublished observations, PD 2022) were abandoned due to technical issues, and determining the local distribution of Arg within solid tumors remains an active line of study. Future work employing cell lines recombinant with Arg inducible promoters controlling expression of fluorescent reporters may offer some insight but would be difficult to quantitatively interpret without orthogonal methods to verify reporter signal with Arg distribution.

Critically, while loss of ASS1 from tumor cells reduced the efficacy of MYXV-based OV, this effect could be partially rescued by arming recombinant viruses with ASS1 (figures 6 and 7). Interestingly, it is unclear how the increased viral replication seen in ASS1-expressing MYXV constructs results in improved tumor control. The most obvious model is that increased viral replication causes more direct viral lysis of infected tumors cells. This model, however, is difficult to rationalize with the observation that the total amount of MYXV infection within a tumor rarely exceeds ~5% to 10% even in ASS1-competent settings. An alternative model might be presented by the recent observation that the induction of the antitumor immune responses required to cause tumor regression in MYXV-based OV likely represents thresholded events.[28] In this model, the increased replication observed for ASS1-expressing viruses allows them to cross a defined threshold which then induces a better therapeutic response. Third, this effect could also be explained by more robust expression of a recombinant virus's therapeutic transgenes. For example, increased replication of MyxAss1/PD1/IL-12 could result in locally increased concentrations of IL-12 which render the treatment more effective. Finally, decreased consumption of bioavailable Arg resulting from viral reconstitution of

Arg biosynthesis may also liberate Arg content for use by other cells, such as T cells, that depend on Arg for proper function.[45] Nonetheless, viral reconstitution of ASS1 clearly improved therapeutic outcomes in the ASS1-deficient model, and future research will be required to definitively determine the mechanism at hand.

Ultimately, our results demonstrate that considering changes to tumor metabolism in the context of OV performance is a worthwhile endeavor, particularly for metabolic dysregulations that are as highly penetrant as the loss of ASS1. Compared with normal tissues, numerous metabolites have been experimentally shown to be altered within the TME. Though our current studies focus on the role of Arg and ASS1 competency in the replication of MYXV, it is highly likely that changes to other metabolites can influence viral replication within the context of OV. Identifying how these changes affect both the quality of viral infection and the subsequent antitumor immune response may provide additional strategies to improve the therapeutic efficacy of OV and is therefore deserving of further study.

Acknowledgements The authors thank the Metabolomics Core Facility at Robert H. Lurie Comprehensive Cancer Center of Northwestern University for providing the metabolomics services.

Contributors PD generated recombinant viruses, performed experiments, analyzed the data, and prepared the manuscript. HC performed the experiments. MYB generated the recombinant viruses. EB designed the experiments, oversaw the project, prepared the manuscript, and acts as gurantor.

Funding This work was funded by grants to EB from NIH-NCI (R01-CA194090 and R21-CA268163), NIH-NIAID (R21-AI142387), and the ACS (RSG-17-047-01-MPC), as well as grants from the UNM Comprehensive Cancer Center (P30-CA118100).

Competing interests EB holds intellectual property rights to recombinant oncolytic viruses encoding argininosuccinate synthetase 1 as well as intellectual property rights to recombinant oncolytic myxoma virus (MYXV) encoding soluble PD1 and interleukin-12. EB also holds intellectual property rights to a variety of other recombinant oncolytic MYXVs which are not relevant to the current article.

Patient consent for publication Not applicable.

Ethics approval Not applicable.

Provenance and peer review Not commissioned; externally peer reviewed.

Data availability statement Data are available upon reasonable request. No large clinical datasets are presented in the current article. All materials needed to reproduce the current experiments are commercially available or will be shared with other investigators. Metabolomics data are freely available upon request.

ORCID iD

Eric Bartee http://orcid.org/0000-0003-1793-446X

REFERENCES

1 Kaufman HL, Kohlhapp FJ, Zloza A. Oncolytic viruses: a new class of immunotherapy drugs. *Nat Rev Drug Discov* 2015;14:642–62.
2 Moreno-Altamirano MMB, Kolstoe SE, Sánchez-García FJ. Virus control of cell metabolism for replication and evasion of host immune responses. *Front Cell Infect Microbiol* 2019;9:95.
3 Sanchez EL, Lagunoff M. Viral activation of cellular metabolism. *Virology* 2015;479–480:609–18.
4 Sumbria D, Berber E, Mathayan M, *et al*. Virus infections and host metabolism—can we manage the interactions? *Front Immunol* 2020;11:594963.
5 Thaker SK, Ch'ng J, Christofk HR. Viral hijacking of cellular metabolism. *BMC Biol* 2019;17:59.
6 Zandi M, Shokri S, Mahmoudvand S, *et al*. Interplay between cellular metabolism and DNA viruses. *J Med Virol* 2022;94:5163–73.
7 Yu Y, Maguire TG, Alwine JC. Human cytomegalovirus activates glucose transporter 4 expression to increase glucose uptake during infection. *J Virol* 2011;85:1573–80.
8 Thai M, Thaker SK, Feng J, *et al*. MYC-induced reprogramming of glutamine catabolism supports optimal virus replication. *Nat Commun* 2015;6:8873.
9 Martínez-Reyes I, Chandel NS. Cancer metabolism: looking forward. *Nat Rev Cancer* 2021;21:669–80.
10 Pavlova NN, Thompson CB. The emerging hallmarks of cancer metabolism. *Cell Metab* 2016;23:27–47.
11 DeBerardinis RJ, Chandel NS. Fundamentals of cancer metabolism. *Sci Adv* 2016;2:e1600200.
12 Hanahan D, Weinberg RA. Hallmarks of cancer: the next generation. *Cell* 2011;144:646–74.
13 Dillon BJ, Prieto VG, Curley SA, *et al*. Incidence and distribution of argininosuccinate synthetase deficiency in human cancers. *Cancer* 2004;100:826–33.
14 Eisenbach L, Segal S, Feldman M. MHC imbalance and metastatic spread in Lewis lung carcinoma clones. *Int J Cancer* 1983;32:113–20.
15 Bartee MY, Dryja PC, Bartee E. Chimeric tumor modeling reveals role of partial PDL1 expression in resistance to virally induced immunotherapy. *J Immunother Cancer* 2019;7:11.
16 Bartee MY, Dunlap KM, Bartee E. Tumor-localized secretion of soluble PD1 enhances oncolytic virotherapy. *Cancer Res* 2017;77:2952–63.
17 Stanford MM, Shaban M, Barrett JW, *et al*. Myxoma virus oncolysis of primary and metastatic B16F10 mouse tumors in vivo. *Mol Ther* 2008;16:52–9.
18 Rahman MM, McFadden G. Oncolytic virotherapy with myxoma virus. *J Clin Med* 2020;9:171.
19 Valenzuela-Cardenas M, Gowan C, Dryja P, *et al*. TNF blockade enhances the efficacy of myxoma virus-based oncolytic virotherapy. *J Immunother Cancer* 2022;10:e004770.
20 Smallwood SE, Rahman MM, Smith DW, *et al*. Myxoma virus: propagation, purification, quantification, and storage. *Curr Protoc Microbiol* 2010;Chapter 14:Unit 14A.1.
21 Schindelin J, Arganda-Carreras I, Frise E, *et al*. Fiji: an open-source platform for biological-image analysis. *Nat Methods* 2012;9:676–82.
22 Weinberg SE, Singer BD, Steinert EM, *et al*. Mitochondrial complex III is essential for suppressive function of regulatory T cells. *Nature* 2019;565:495–9.
23 Xia J, Psychogios N, Young N, *et al*. Metaboanalyst: a web server for Metabolomic data analysis and interpretation. *Nucleic Acids Res* 2009;37:W652–60.
24 Luiking YC, Hallemeesch MM, Vissers YLJ, *et al*. In vivo whole body and organ arginine metabolism during endotoxemia (sepsis) is dependent on mouse strain and gender. *J Nutr* 2004;134:2768S–2774S.
25 Nieves C Jr, Sitren HS, Herrlinger-Garcia KA, *et al*. Pharmacologic levels of dietary arginine in CB6F1 mice increase serum ammonia in the healthy state and serum nitrite in endotoxemia. *JPEN J Parenter Enteral Nutr* 2007;31:101–8.
26 Marini JC, Didelija IC, Castillo L, *et al*. Plasma arginine and ornithine are the main citrulline precursors in mice infused with arginine-free diets. *J Nutr* 2010;140:1432–7.
27 Doty RA, Liu J, McFadden G, *et al*. Histological evaluation of Intratumoral Myxoma virus treatment in an immunocompetent mouse model of Melanoma. *Oncolytic Virother* 2013;2:1–17.
28 Flores EB, Aksoy BA, Bartee E. Initial dose of oncolytic myxoma virus programs durable antitumor immunity independent of in vivo viral replication. *J Immunother Cancer* 2020;8:e000804.
29 Zemp FJ, Lun X, McKenzie BA, *et al*. Treating brain tumor-initiating cells using a combination of myxoma virus and rapamycin. *Neuro Oncol* 2013;15:904–20.

30 Pisklakova A, McKenzie B, Zemp F, *et al*. M011L-deficient oncolytic myxoma virus induces apoptosis in brain tumor-initiating cells and enhances survival in a novel immunocompetent mouse model of glioblastoma. *Neuro Oncol* 2016;18:1088–98.
31 Zheng M, Huang J, Tong A, *et al*. Oncolytic viruses for cancer therapy: barriers and recent advances. *Mol Ther Oncolytics* 2019;15:234–47.
32 Shin DH, Nguyen T, Ozpolat B, *et al*. Current strategies to circumvent the antiviral immunity to optimize cancer virotherapy. *J Immunother Cancer* 2021;9:e002086.
33 Kellish P, Shabashvili D, Rahman MM, *et al*. Oncolytic Virotherapy for small-cell lung cancer induces immune infiltration and prolongs survival. *J Clin Invest* 2019;129:2279–92.
34 Mahar R, Ragavan M, Chang MC, *et al*. Metabolic signatures associated with oncolytic myxoma viral infections. *Sci Rep* 2022;12:12599.
35 Archard LC, Williamson JD. The effect of arginine deprivation on the replication of vaccinia virus. *J Gen Virol* 1971;12:249–58.
36 Osborn JGE, Chesters PM, Williamson JD. Arginine metabolism in infected cell cultures as a marker character for the differentiation of Orthopoxviruses. *J Hyg* 1984;93:213–23.
37 Jin H-O, Hong S-E, Kim J-Y, *et al*. Amino acid deprivation induces AKT activation by inducing GCN2/ATF4/REDD1 axis. *Cell Death Dis* 2021;12:1127.
38 Harding HP, Ordonez A, Allen F, *et al*. The ribosomal P-stalk couples amino acid starvation to GCN2 activation in mammalian cells. *eLife* 2019;8:e50149.
39 Dauber B, Wolff T. Activation of the antiviral kinase PKR and viral countermeasures. *Viruses* 2009;1:523–44.
40 Berlanga JJ, Ventoso I, Harding HP, *et al*. Antiviral effect of the mammalian translation initiation factor 2alpha kinase GCN2 against RNA viruses. *EMBO J* 2006;25:1730–40.
41 del Pino J, Jiménez JL, Ventoso I, *et al*. GCN2 has inhibitory effect on human immunodeficiency virus-1 protein synthesis and is cleaved upon viral infection. *PLoS One* 2012;7:e47272.
42 Krishnamoorthy J, Mounir Z, Raven JF, *et al*. The eIF2alpha kinases inhibit vesicular stomatitis virus replication independently of eIF2alpha phosphorylation. *Cell Cycle* 2008;7:2346–51.
43 Liu Y, Wang M, Cheng A, *et al*. The role of host eIF2α in viral infection. *Virol J* 2020;17:112.
44 Ye J, Palm W, Peng M, *et al*. GCN2 sustains mTORC1 suppression upon amino acid deprivation by inducing Sestrin2. *Genes Dev* 2015;29:2331–6.
45 Geiger R, Rieckmann JC, Wolf T, *et al*. L-arginine modulates T cell metabolism and enhances survival and anti-tumor activity. *Cell* 2016;167:829–42.